Cell Chemical Biology, Volume *29*

Supplemental information

Acriflavine, a clinically approved drug, inhibits SARS-CoV-2 and other betacoronaviruses

Valeria Napolitano, Agnieszka Dabrowska, Kenji Schorpp, André Mourão, Emilia Barreto-Duran, Malgorzata Benedyk, Pawel Botwina, Stefanie Brandner, Mark Bostock, Yuliya Chykunova, Anna Czarna, Grzegorz Dubin, Tony Fröhlich, Michael Hölscher, Malwina Jedrysik, Alex Matsuda, Katarzyna Owczarek, Magdalena Pachota, Oliver Plettenburg, Jan Potempa, Ina Rothenaigner, Florian Schlauderer, Klaudia Slysz, Artur Szczepanski, Kristin Greve-Isdahl Mohn, Bjorn Blomberg, Michael Sattler, Kamyar Hadian, Grzegorz Maria Popowicz, and Krzysztof Pyrc

SUPPLEMENTARY FIGURES

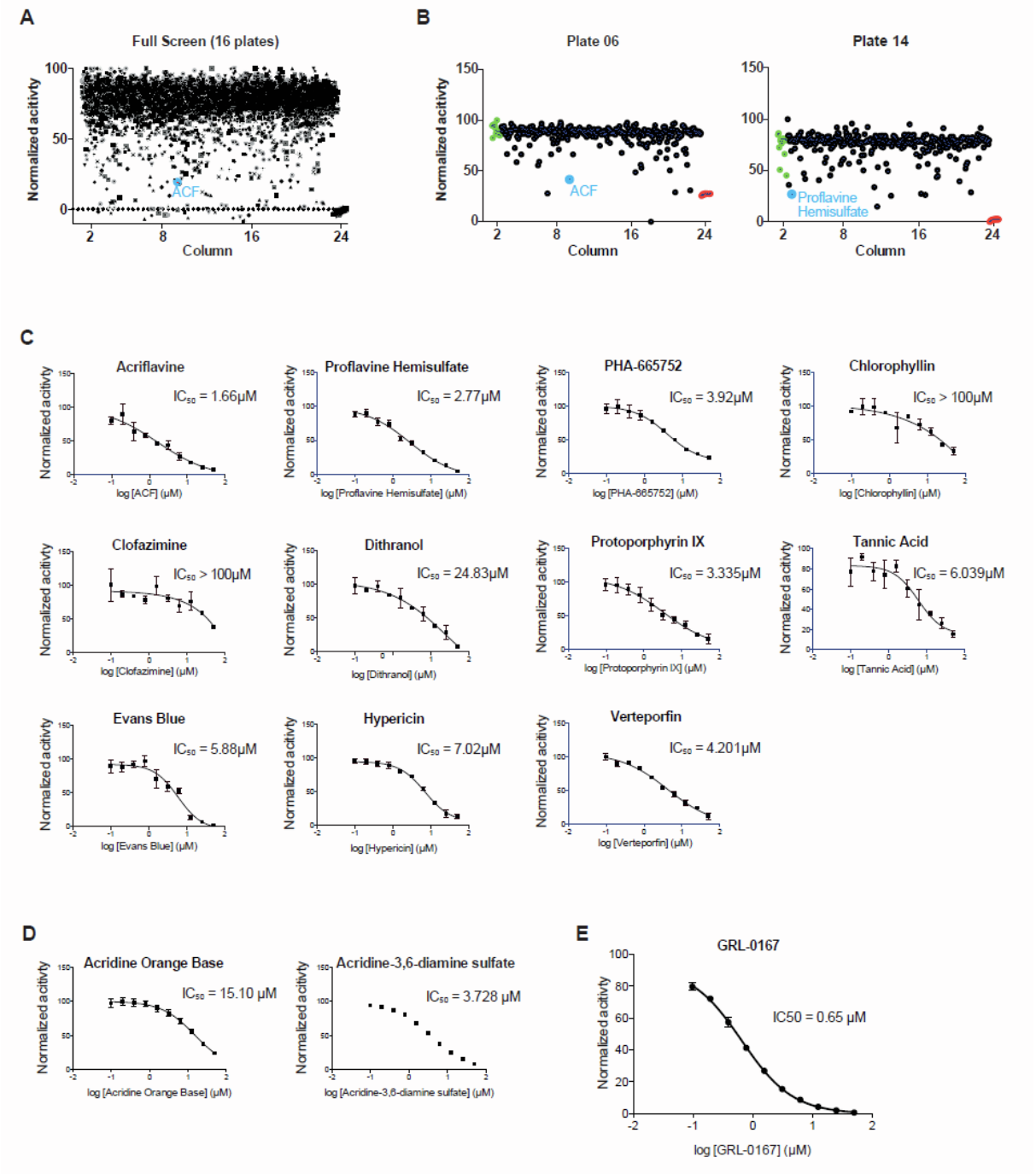

Figure S1. High-throughput screening, Related to Figure 1 (A) Summary of the high-throughput screening campaign (16 x 384-well plates). RLRGG-AMC peptide was used as a substrate for His-PL^{pro}. Each dot represents the data of one compound in one well (n = 1). Controls without protease are located in column 24, and ACF as a representative hit is depicted in blue. **(B)** Two representative screening plates with ACF and Proflavine Hemisulfate as hits (blue) are depicted side by side. **(C)** Dose-response curves of eleven hits. These hits were re-ordered and re-tested in ten-point titrations on the primary screening assay (mean ± SD, n = 2). Shown are inhibition curves and IC_{50} values. **(D)** as in **(C)**. Analogs of ACF were tested in ten-point titrations on the primary assay (mean ± SD, n = 3). **(E)** Inhibition curve of the known PL^{pro} inhibitor GLR-0617 (mean ± SD, n = 3).

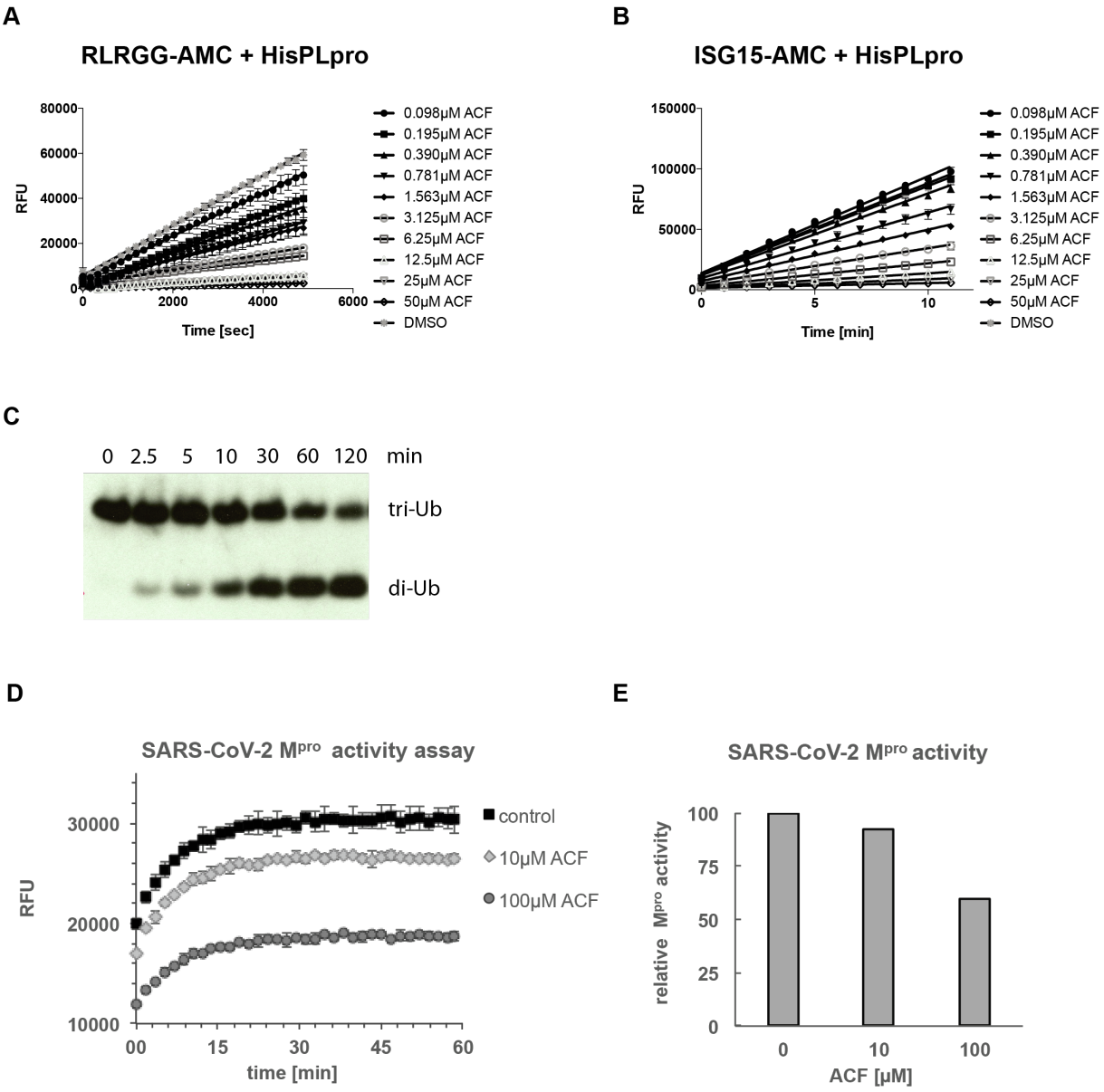

Figure S2. PL^{pro} and M^{pro} cleavage assays, Related to Figure 1 (A) and **(B)** Kinetic assays of His-PL^{pro} activity in the presence of different concentrations of ACF. RLRGG-AMC in **(A)** and ISG15-AMC in **(B)** were used as substrates. Reactions were performed in triplicates. **(C)** Time-course analysis of tri-ubiquitin K48-linked (2 μM) hydrolysis using 100 nM His-PL^{pro} **(D)** The digestion of fluorogenic substrate was recorded in the absence and presence of ACF. The vertical shift in signal levels is caused by ACF absorbance. **(E)**. Only a small decrease of M^{pro} activity is observed at a physiologically irrelevant ACF concentration of 100 μM.

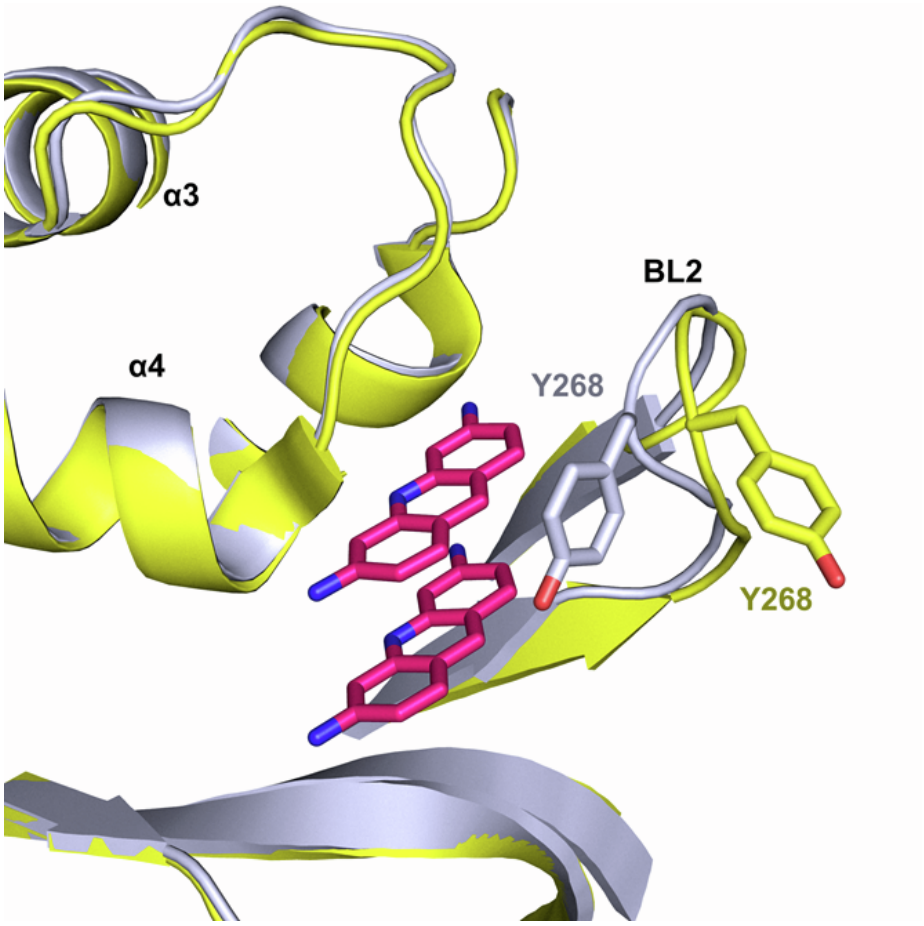

Figure S3. Comparison of SARS-CoV2-PL^{pro} in the proflavine-bound and apo-state, Related to Figure 2. Bound PL^{pro} is colored in gray; whereas the unbound PL^{pro} (PDB ID: 7D47) is colored in yellow. The BL2 loop is involved in an induced-fit rearrangement upon the binding mostly due to the movement of the Tyr268. The side-chain of Tyr268 participates in a π-π stacking with proflavine molecules.

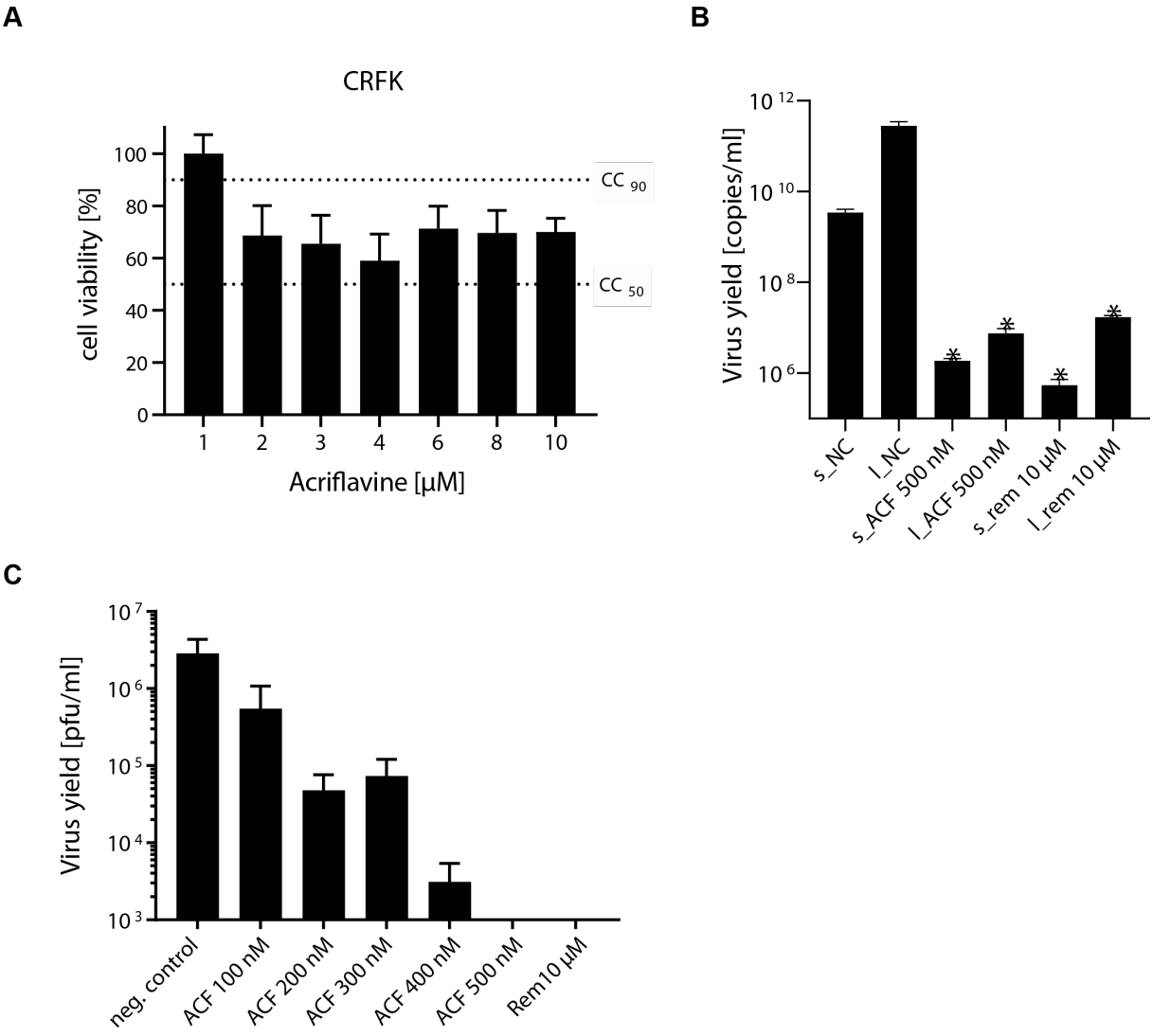

Supplementary Figure S4. Cell-based assays with ACF, Related to Figure 3. (A) The cytotoxicity of ACF in CRFK cells. **(B)** ACF Inhibits intracellular replication of SARS-CoV-2 *in vitro* in Vero cells. The figure shows RT-qPCR analysis of cell culture supernatants and lysates infected with SARS-CoV-2 at 1600 $TCID_{50}$/ml 24 h post-infection. The experiment was performed in triplicate. s_: supernatants; l_: cel lysates. NC: non-treated control, rem: remdesivir. The results are presented as average values with standard deviations (error bars). An asterisk indicates values that are significantly different from the control ($p< 0.05$). **(C)** Inhibition of virus replication by ACF in Vero cells. Inhibition of viral replication in Vero cells by ACF was evaluated with the plaque assay and is presented as change of titer.

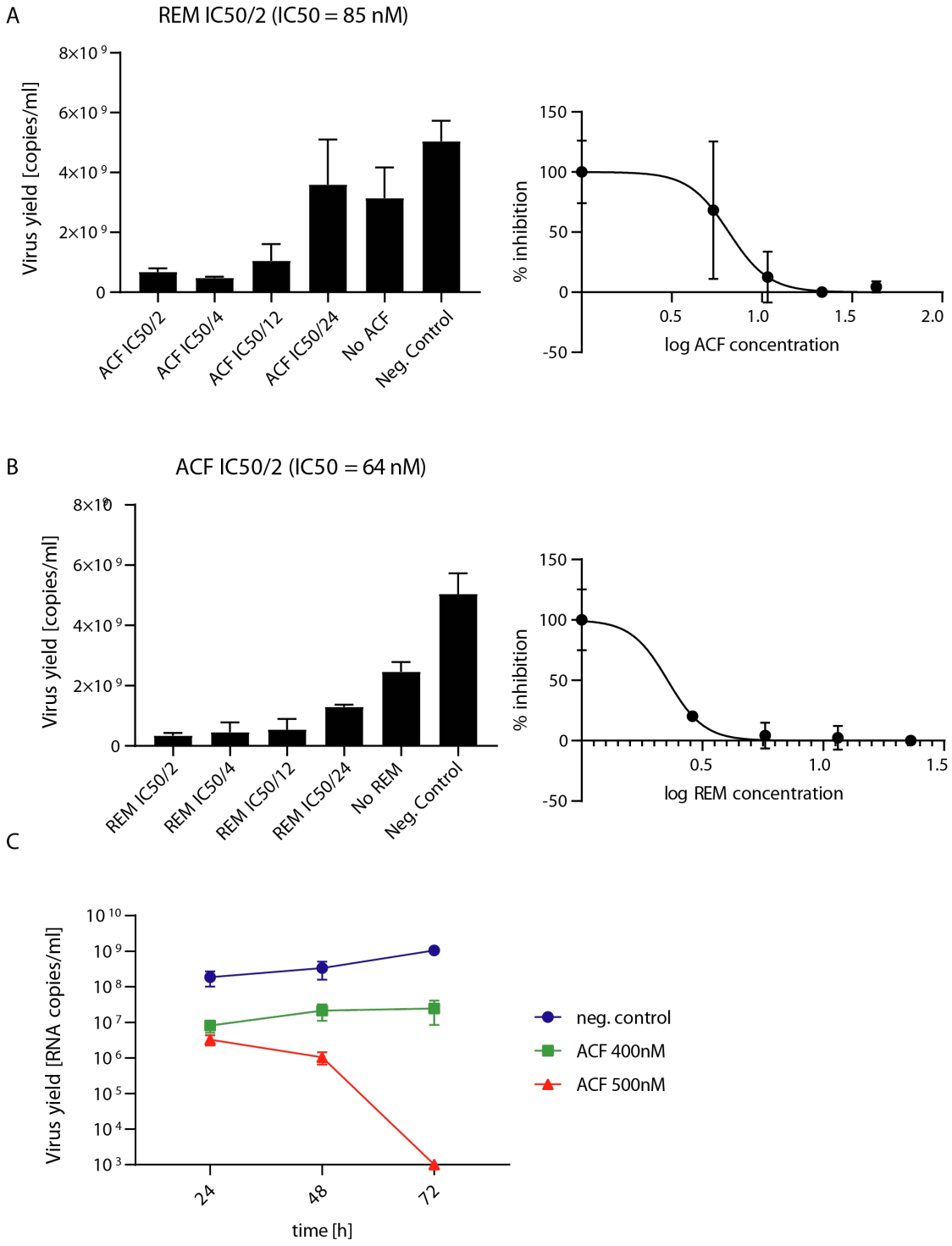

Supplementary Figure S5. Synergistic effect of ACF and remdesivir, Related to Figure 4. Inhibition of virus replication by ACF and remdesivir (REM) in Vero cells. The figure shows qRT-PCR analyses carried out 48 h post-infection of cell culture supernatants from cultures infected with SARS-CoV-2 at 1600 TCID50/ml. (**A**) Inhibition of virus with constant concentration of remdesivir with decreasing concentration of ACF. (**B**) Inhibition of virus with constant concentration of ACF with decreasing concentration of remdesivir. **(C)** ACF blocks SARS-CoV-2 replication *in vitro* and *ex vivo.* Antiviral activity of ACF against SARS-CoV-2 in human airway epithelium (prepared in-house). The figure shows RT-qPCR analysis of HAE culture supernatants infected with SARS-CoV-2. The assay was performed at least in duplicate, and median values with range are presented. Two-way ANOVA analysis with Dunnett's post-hoc test indicated that ACF and REM significantly inhibit virus yields during infection course compared to untreated control.

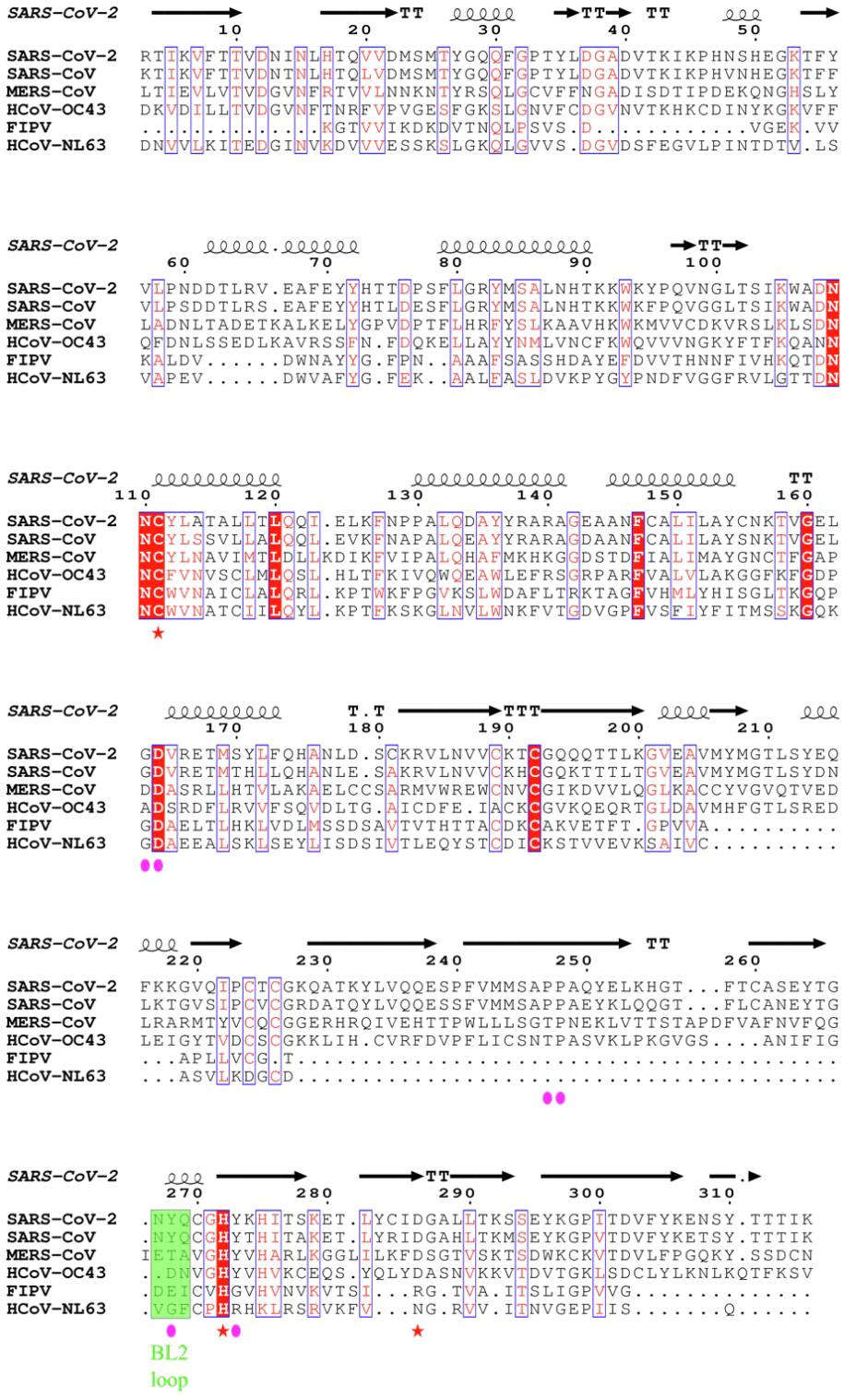

Supplementary Figure S6. Multiple sequence alignment for PL^{pro} from selected alpha- and beta-coronaviruses, Related to Figure 5. The multiple sequence alignment was generated with ESPript3 (Robert and Gouet, 2014). Residues with high SimilarityGlobalScore are highlighted as red characters on a white background or white characters on a red background (if residues are strictly conserved in the column) with blue frames. Residues from BL2 loop are marked in green. A red star indicates the catalytic residues. Purple circles indicate residues involved in the recognition of the proflavine I and proflavine II molecules. These latter vary between alpha- and beta-coronaviruses especially for concerning the amino acids contacting proflavine I, which may rationalize why ACF does not inhibit PL^{pro} from alphacoronaviruses (FIPV, HCoV-NL63).

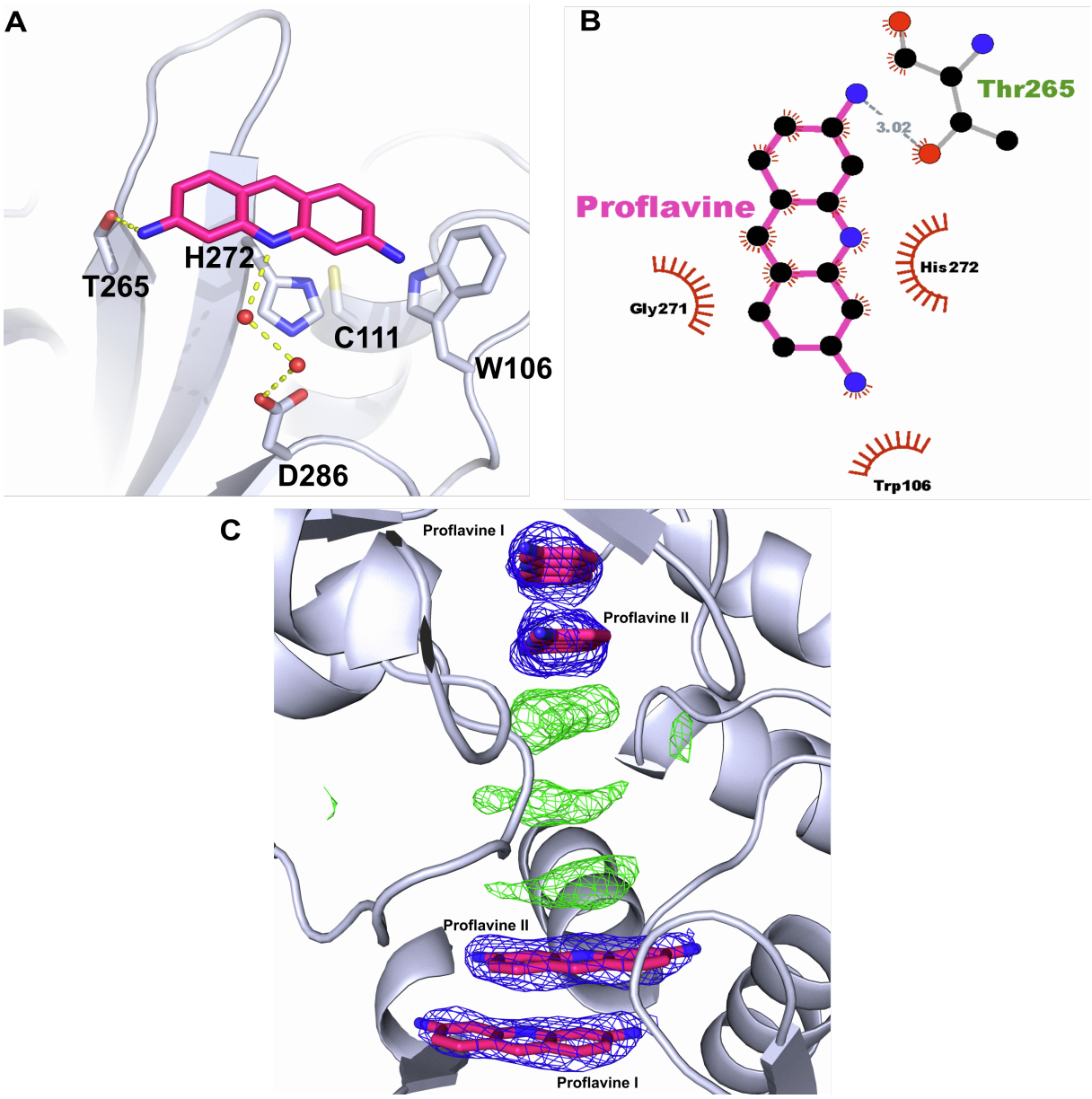

Supplementary Figure S7. Proflavine molecule at the interface between SARS-CoV2-PL^{pro} asymmetric units, Related to Figure 2. (A) Most probably due to a crystal packing molecule of proflavine was found on top of the catalytic triad (C111, H272, D286). Important residues are highlighted as stick model. Two water molecules (red spheres) mediate a hydrogen bond with D286. Hydrogen bonds are represented as yellow dashed lines. **(B)** 2D plot of the molecular interactions between proflavine and the residues of SARS-CoV-2-PL^{pro}. **(C)** Electron density map showing the fractional presence of additional aromatic proflavine-like molecules π-π stacked one on top of the other between two copies of SARS-CoV2-PL^{pro} present in the crystal lattice. $2F_o$-F_c electron density map is contoured at 2σ. The electron density of the identified proflavine molecules is colored in blue; whereas additional electron density is colored in green. The densities are most likely caused by weak and transiently-bound proflavines. We did not model them in the crystal structure as their electron density was much weaker than active site-bound molecules

SUPPLEMENTARY TABLES

Supplementary Table S1.
Compounds selected from the library for validation as PL^{pro} inhibitors, Related to Figure S1.

no	Compound
1	Verteporfin
2	Evans Blue
3	Clofazimine
4	Hypericin from *Hypericus perforatum*
5	Dithranol
6	Chlorophyllin sodium copper salt
7	Acriflavine hydrochloride
8	Protoporphyrin IX
9	Tannic acid
10	PHA-665752 hydrate
11	Proflavine hemisulfate salt hydrate

Supplementary Table S2.
Primers and probes used for a RT-qPCR, Related to Figure 3+4+5+7.

Target	Primer	Sequence	Concentration [nM]
SARS-CoV-2	Forward	CAC ATT GGC ACC CGC AAT C	600
	Reverse	GAG GAA CGA GAA GAG GCT TG	800
	Probe	ACT TCC TCA AGG AAC AAC ATT GCC A (FAM / BHQ1)	200
MERS-CoV	Forward	GGG TGT ACC TCT TAA TGC CAA TTC	500
	Reverse	TCT GTC CTG TCT CCG CCA AT	500
	Probe	ACC CCT GCG CAA AAT GCT GGG (FAM / TAMRA)	200
HCoV-NL63	Forward	AAA CCT CGT TGG AAG CGT GT	500
	Reverse	CTG TGG AAA ACC TTT GGC ATC	500
	Probe	TGT TAT TCA GTG CTT TGG TCC TCG TGA T (FAM / TAMRA)	100
FIPV	Forward	TCT CGT GGT CGG AAG AAT AAT G	500
	Reverse	GAA CAA GGT CTC TCG GAC ATA AA	500
	Probe	CCC ATT ACC CTC GAA CAA GGA TCT (FAM/BHQ1)	200
HCoV-OC43	Forward	AGC AAC CAG GCT GAT GTC AAT ACC	500
	Reverse	AGC AGA CCT TCC TGA GCC TTC AAT	500
	Probe	TGA CAT TGT CGA TCG GGA CCC AAG TA (FAM/BHQ1)	200

Supplementary Table S3.
Data collection and refinement statistics, Related to Figure 2.

	SCov2-PLpro-Proflavine (PDB ID:7NT4)
Data collection	
Space group	$P6_522$
Cell dimensions	
a, *b*, *c* (Å)	111.37, 116.37, 253.57
α, β, γ (°)	90, 90, 120
Resolution (Å)	49.4(2.68) *
Wavelength (Å)	1.00
R_{pim}	8.6(46.1)
$I / \sigma I$	51.9(1.8)
Completeness (%)	95.7(72.2)
Redundancy	38.1
Observed reflections	801001 (29586)
Unique reflections	21442 (1073)
Refinement	
Resolution (Å)	40 (2.68)
No. reflections	22325
R_{work} / R_{free}	19.3/ 26.4
No. atoms	
Protein	2
Ligand/ion	6
Water	193
B-factors	
Protein	43.9
Ligand/ion	61.33
Water	25.2
R.m.s. deviations	
Bond lengths (Å)	0.014
Bond angles (°)	2.16
Ramachandran statistics (%)	
Most favored regions	93.3
Additionally allowed regions	5.2
Generously allowed regions	1.5

*A single crystal was used for data collection and structure determination. *Values in parentheses are for highest-resolution shell.

Supplementary Table S4.
ACF IC_{50} values on HAE cultures at different time points, Related to Figure 4.

Time post-infecton	IC_{50}	Log IC_{50}	Std. error (Log IC_{50})
24 h	14.03 nM	1.147	0.83
48 h	12.59 nM	1.100	22.11
72 h	65.85 nM	1.819	1.85
96 h	61.97 nM	1.792	0.85

Supplementary Table S5.
Pharmacokinetic parameters, Related to Figure 6.
Selected pharmacokinetic parameters for ACF components in male CD-1 mice following administration of 15 and 100 mg/kg of ACF hydrochloride IV and PO respectively. ACF is a mixture of four major components; fractional doses are calculated based on composition analysis (see supplementary analysis):

	Sample	Administration/ fractional dose (mg/kg)	Pharmacokinetic Parameters		
			C_{max} (ng/mL)	$AUC_{0\rightarrow t\ min}$ (ng*min/ml)	$T_{1/2}$ (min)
Plasma	ACF	IV / 2.5	205	4870	66.2
		PO / 17	BQL	BQL	ND
	PF	IV / 8.4	1060	43800	102
		PO / 56	461	32700	ND
	Side methylated ACF	IV / 0.6	54.7	1450	61.3
		PO / 4.0	BQL	BQL	ND
	Side methylated PF	IV / 3.3	217	7720	56.1
		PO / 22	60.9	4690	ND
Lungs	ACF	IV / 2.5	7380	574000	332
		PO / 17	1960	7530	ND
	PF	IV / 8.4	43800	1650000	66.5
		PO / 56	14100	1130000	ND
	Side methylated ACF	IV / 0.6	1930	118000	185
		PO / 4.0	460	8380	178
	Side methylated PF	IV / 3.3	15400	445000	50.1
		PO / 22	3590	225000	ND

BLQ – Below the lower limit of quantitation (LLOQ)
ND – Not determined